

# Structure–Property Correlations in Microwave Joining of Inconel 718

AMIT BANSAL,<sup>1,3</sup> APURBBA KUMAR SHARMA,<sup>1,4</sup> PRADEEP KUMAR,<sup>1,5</sup>  
and SHANTANU DAS<sup>2,6</sup>

1.—Department of Mechanical and Industrial Engineering, Indian Institute of Technology Roorkee, Roorkee 247667, India. 2.—Reactor Control Division, BARC, Mumbai 400085, India. 3.—e-mail: amit.bansal978@gmail.com. 4.—e-mail: akshafme@iitr.ac.in. 5.—e-mail: kumarfme@iitr.ac.in. 6.—e-mail: shantanu@barc.gov.in

The butt joining of Inconel 718 plates at 981°C solution treated and aged (981STA) condition was carried out using the microwave hybrid heating technique with Inconel 718 powder as a filler material. The developed joints were free from any microfissures (cracks) and were metallurgically bonded through complete melting of the powder particles. The as-welded joints were subjected to postweld heat treatments, including direct-aged, 981STA and 1080STA. The microstructural features of the welded joints were investigated using a field emission-scanning electron microscope equipped with x-ray elemental analysis. Microhardness and room-temperature tensile properties of the welded joints were evaluated. The postweld heat-treated specimens exhibited higher microhardness and tensile strength than the as-welded specimens due to the formation of strengthening precipitates in the microstructure after postweld heat treatments. The microhardness of the fusion zone of the joint in 1080STA condition was higher than all welded conditions due to the complete dissolution of Laves phase after 1080STA treatment. However, the tensile strength of the welded specimen in 981STA condition was higher than all welded conditions. The tensile strength in 1080STA condition was lower than that in 981STA condition because of the grain coarsening that took place after 1080STA condition. The fractography of the fractured surfaces was carried out to determine the structure–property–fracture correlation.

## INTRODUCTION

Precipitation-hardened Inconel 718 is widely used in high-temperature applications including aircraft engine components, i.e., critical rotating parts, airfoils, supporting structure, and industrial gas turbine engines because of its excellent high-temperature strength, corrosion resistance, and good fatigue life at temperatures up to 650°C. This alloy also exhibits high strength at cryogenic temperature.<sup>1</sup> Prior to the introduction of Inconel 718 in the year 1959, the strengthening of the Ni-based superalloy was attributed to precipitation of aluminum (Al) and titanium (Ti) compounds. The precipitation of Al and Ti is denoted by Ni<sub>3</sub>(Al, Ti) and is abbreviated by  $\gamma'$ . The precipitation of  $\gamma'$  depletes the surrounding  $\gamma$  matrix of Al and Ti, and it results

in a decrease in the lattice parameter of the matrix. This decrease produces aging contraction, which promotes the chances of postweld heat treatment cracking because the strain produced hinders the relaxation of residual stress in the heat-affected zone (HAZ).<sup>2</sup> However, Inconel 718 uses the niobium (Nb) as the primary strengthening element, and  $\gamma''$  (an ordered body-centered tetragonal intermetallic compound of composition Ni<sub>3</sub>Nb), rather than the  $\gamma'$ , is responsible for precipitation hardening during aging. The  $\gamma''$  ages much slower than the  $\gamma'$ ; hence, it reduces the problem of postweld heat-treatment cracking. The volume fraction of  $\gamma''$  and  $\gamma'$  in the  $\gamma$  matrix is approximately 16% and 4%, respectively, after a full heat treatment.<sup>3,4</sup> Basically, Inconel 718 material was specifically designed to overcome the problem of postweld heat-treatment

cracking. Thus, Inconel 718 exhibits good weldability due to its resistance to strain age cracking. However, the addition of Nb reduces the strain age cracking problem, but it produces the problem of microfissure (liquation cracking) in the HAZ during welding.

Inconel 718 material is usually welded by the fusion welding process. The most commonly used fusion welding processes are tungsten inert gas welding (TIG), electron beam welding (EBW), laser beam welding (LBW), and plasma arc welding. The microfissure (liquation cracking) takes place due to a combined action of the grain boundary location and tensile stress. The other problem is that because Nb is a high-concentration refractory element, it segregates easily during solidification. As a result, the formation of Nb-rich Laves phase takes place. Laves phase is a brittle intermetallic compound that is represented as  $(\text{Ni, Cr, Fe})_2(\text{Nb, Mo, Ti})$  in the interdendritic regions during weld metal solidification. Previous investigations show that the formation of Laves phase is detrimental to weld mechanical properties because (I) it forms a weak zone of microstructure between the Laves phase and matrix by consuming a significant amount of useful alloying elements, (II) it promotes the hot cracking in Inconel 718 due to its low melting point, and (III) it is detrimental to the weld mechanical properties such as tensile ductility, fracture toughness, fatigue, and creep properties.<sup>5–10</sup> Thus, it is necessary to reduce the Laves phase and to develop the uniform homogenized microstructure. It has been reported that the morphology and composition of Laves phase are strongly dependent on the heat input and cooling rate of the welding process.<sup>9</sup> Laves phase can be reduced by decreasing the segregation of Nb during weld metal solidification. The segregation, on the other hand, can be reduced by using a low heat input or fast cooling rate welding process. Ram et al.<sup>3</sup> used the electron beam oscillation technique for reducing the Nb segregation and Laves formation in Inconel 718. The fast cooling rate exhibited by laser welding reduces the problem of Nb segregation in Inconel 718 weld, but the fast cooling rate in laser welding produces the microfissures in the HAZ.<sup>11,12</sup> The microwave processing of materials is gaining popularity due to its specific characteristics such as rapid heating and increased productivity. Furthermore, in many cases the microwave-processed products exhibit superior properties to those obtained by conventional processing. In microwave heating, the material is heated at a molecular level due to dipole rotation and ionic conduction. Hence, there is an energy conversion rather than energy transfer, which generally occurs in the conventional processing of materials. However, the metallic materials are difficult to process using microwave energy because they reflect microwave at room temperature because of their low skin depth.<sup>13,14</sup> However, Roy et al.<sup>15</sup> reported that in powdered form, all metals and alloys can be heated both efficiently and effectively using

microwave energy. Furthermore, the microwave joining of bulk metallic materials was reported by Sharma et al.<sup>16</sup> Srinath et al.<sup>17–19</sup> reported joining of similar as well as dissimilar materials using microwave hybrid heating (MHH) technique. The microwave processing of materials is environment friendly. In the current work, butt joining of Inconel 718 plates was carried out by using Inconel 718 powder as a filler material in an industrial microwave oven. However, it is difficult to control the segregation of refractory elements such as Nb and Mo, which results in the formation of Laves phase in the joint zone (fusion zone) during the MHH process. Thus, the joints were subjected to three different postweld heat treatments, including direct aged (DA), 981°C solution treated and aged (981STA), and 1080°C solution treated and aged (1080STA). The influence of postweld heat treatment is investigated in the microstructure developed in the fusion zone of joint formed by the MHH process, and the mechanical properties of the welded specimens were compared in relation to their microstructure features.

## EXPERIMENTAL PROCEDURE

The following section describes the experimental procedure adopted for butt joining of Inconel 718 plates and various characterizations of the developed joints.

### Material Detail

Commercially available Inconel 718 alloy and Inconel 718 powder was used for the trails. The chemical compositions of the base material and powder material (provided by the suppliers) are given in Table I. Inconel 718 plates with dimensions of  $(30 \times 10 \times 4)$  mm<sup>3</sup> in 981STA condition were used. During solution treatment, the alloy was heated near to the solidus temperature at which the soluble constituents get dissolved to form a solid solution by diffusion and then holding the alloy at that temperature for sufficient time so that complete diffusion occurs, i.e., the homogenized microstructure is formed. The aging was done to obtain the desired strength and hardness of the material. It consists of following steps: (I) solution at 720°C for 8 h, furnace cooled to 620°C in 30 min, hold at 620°C for 8 h, and then air cooling to room temperature. In the current study, Inconel 718 powder with an average particle size of approximately 30  $\mu\text{m}$  was used as a filler material. The powder particles are mainly spherical in shape as shown in Fig. 1. The phase analysis of the powder was carried out using x-ray diffraction (XRD) by Cu-K $\alpha$  radiation. The scan rate used was 0.5° min<sup>-1</sup> and scan range was maintained at 10° to 90°. A typical XRD spectrum of the Inconel 718 powder used as an interfacing material is shown in Fig. 2. The XRD spectrum of Inconel 718 powder is coincident with solid solution of Ni-Cr-based ( $a = 0.359$  nm, space group Fm-3 m) face-centered-cubic (fcc) austenite ( $\gamma$ ) matrix.

**Table I. Chemical composition in wt.% of the materials used**

Material	Elements PRESENT (wt.%)											
	Fe	Ni	Cr	Mo	P	Si	S	C	Nb	Ti	Al	B
Inconel 718 plates	Bal	52.6	17.7	3.13	0.005	0.03	0.002	0.02	5.08	0.97	0.51	0.003
Inconel 718 powder	Bal	53.5	17.7	2.92	0.005	0.03	0.002	0.02	5.215	0.97	0.55	0.003

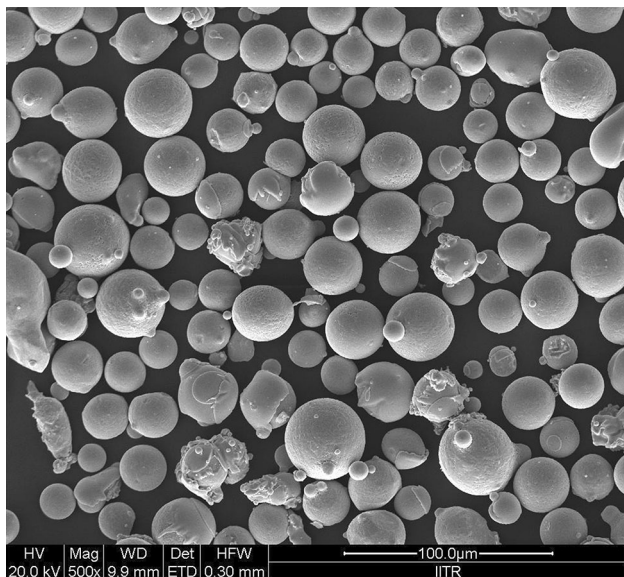


Fig. 1. Typical SEM image illustrating the morphology of the Inconel 718 powder.

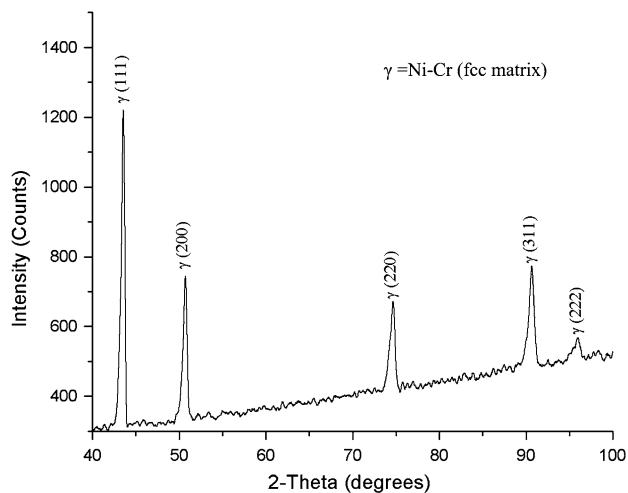


Fig. 2. A typical XRD spectrum of Inconel 718 powder used as an interface layer.

### Base Material Microstructure

The microstructural characterization of the base materials was carried out through field emission-scanning electron microscopy (FE-SEM) and an optical microscope. Figure 3a illustrates the SEM

micrograph of the base material used in 981STA condition, which consisted of the austenite grains with small amounts of randomly distributed white and black particles. FE-SEM equipped with an energy-dispersive x-ray spectroscopy (EDS) was used to determine the chemical composition of these particles. Points 1 and 2 as shown in Fig. 3a indicate the location where chemical analysis was carried out and corresponding EDS spectra are shown in Fig. 3b and c, respectively. From Fig. 3b, it has been found that the white particles represent Nb-rich Laves phase and black particles (Fig. 3c) represent the MC type of carbides, where M represents large Nb, Ti, and Mo metallic atoms.<sup>20</sup> The optical micrographs of the base material in the 981STA and 1080STA conditions are shown in Fig. 4a and b, respectively. It is shown in Fig. 4b that the average grain size in 1080STA condition is significantly larger than that in 981STA condition. Thus, the 1080STA condition results in grain coarsening of the material, which deteriorates the mechanical properties of the base material.

### Developments of Joints

The base materials used in the current work were cleaned with acetone in an ultrasonic cleaner and finally hot dried prior to joining. It was very difficult to keep the dry powder in between the vertical interfacing surfaces of the substrates in the butt configuration to be joined. Thus, a slurry was prepared by mixing the starting powder with a chemical-neutral epoxy resin (Bisphenol-A, Blummer 1450 XX; Bluebell Polymers, Gujarat, India). The prepared slurry was easily placed between the interfacing surfaces to be joined. The slurry evaporates at high temperature (>400°C), and subsequently the void spaces were filled with molten powder particles. Therefore, the slurry has no effect on the joint properties. The whole assembly was kept on an alumina plate, which was further placed into the hot zone of the refractory insulating box (Enerzi Microwave Systems Pvt. Ltd., Karnataka, India). The refractory box was further kept in an industrial microwave oven (Enerzi Microwave Systems Pvt. Ltd.), and it was exposed to microwave radiation at a fixed frequency of 2.45 GHz and 1.1 kW power. The microwave processing parameters used in the current trials are given in Table II. The refractory box was made from a material (high-density alumina board with ceramic wool jackets)

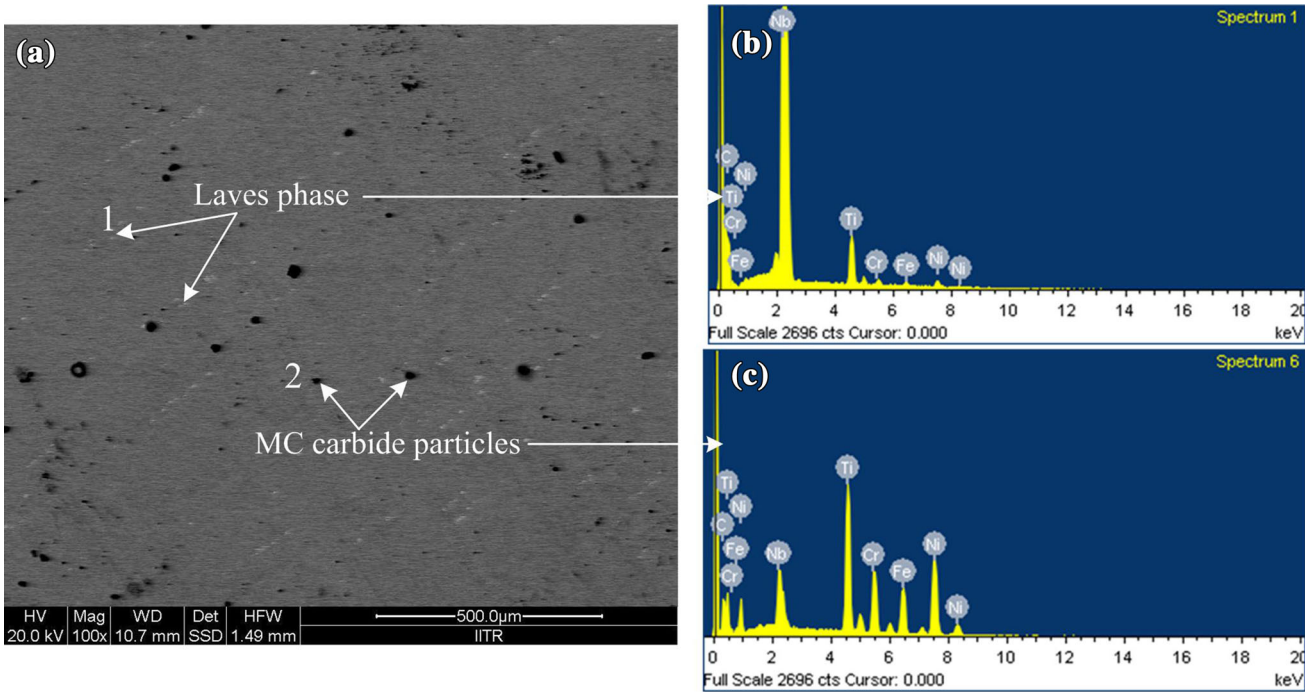


Fig. 3. The SEM micrograph of the base material in 981STA condition and (b, c) EDS spectra at locations 1 and 2, respectively.

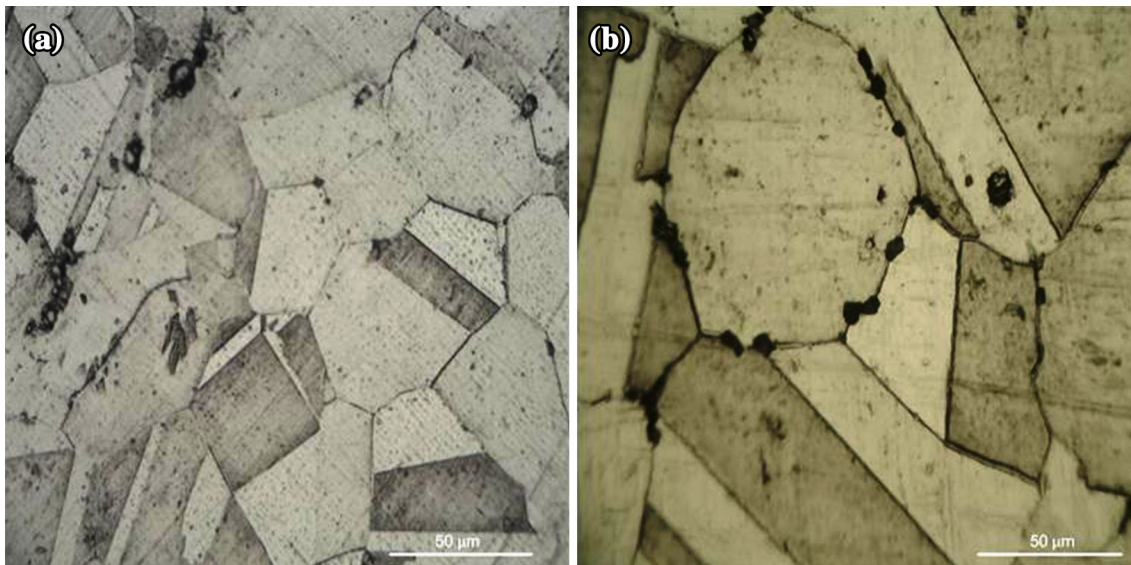


Fig. 4. Optical micrographs of the base material in (a) 981STA condition and (b) 1080STA condition.

with a low dielectric loss. Thus, microwaves can pass through it without any interaction. Inconel 718 material has high oxidation resistance at high temperatures due to presence of elements such as Al, Ti, and Cr. During heating, these elements form a stable passive oxide layer protecting the surfaces from further attack. This stable oxide layer also prevents the wetting of the interfacing surfaces to be joined. Hence, to prevent or minimize oxidation, the experiments were carried out in a vacuum of  $10^{-2}$  bar. However, the vacuum available in the

system was found inadequate to prevent the oxidation of Inconel 718 plates. Hence, to prevent the formation of an oxide layer on the interfacing surfaces, the flux 420 TT (Composition:  $\text{SiO}_2 + \text{TiO}_2$  (wt.% 15),  $\text{CaO} + \text{MgO}$  (wt.% 35),  $\text{Al}_2\text{O}_3 + \text{MnO}$  (wt.% 21),  $\text{CaF}_2$  (wt.% 25)) was applied over the fusion zone. The flux dissolves the oxide layer and prevents further formation of oxide layer on the interfacing surfaces of Inconel 718 to be joined at a high temperature. The skin depth of Ni, the major constituent of the Inconel 718, was calculated to be

0.12  $\mu\text{m}$  at 2.45 GHz frequency, which is significantly less than the powder particle size ( $\sim 30 \mu\text{m}$ ) used in the current study.<sup>14</sup> Hence, the powder particles do not couple well with microwave radiation at room temperature. To overcome this problem, the principles of MHH were applied, in which a suitable susceptor (charcoal powder) was used for increasing the temperature of the powder particle beyond the critical temperature, where the powder particles itself start absorbing microwave radiation. The schematic of the MHH setup used for joining the superalloy is shown in Fig. 5. As the microwave exposure begins, the susceptor easily couples with microwave radiation and it transfers heat to the powder particle through flux by conventional modes of heat transfer. The flux also prevents the contamination of the fusion zone with the susceptor powder. The Inconel 718 powder particles start absorbing microwave radiation at high temperature due to their increased skin depth. The powder particles are melted along with the flux at a high temperature. The melted flux forms slag on the fusion zone and the slag retards the cooling rate, which in turn prevents the microfissures in the fusion zone and the HAZ. On cooling, the slag was removed manually from the fusion zone and the

solidified powder layer becomes the weld bead of the joined pieces. The welded joints were subjected to three different postheat treatments for improving their mechanical properties with precipitation of strengthening phases. These postweld heat treatments are (I) DA, in which welded joints were subjected to aging heat treatment as described in the Material Detail section; (II) solution treatment at 981°C for 30 min and then air cooling to room temperature followed by aging as described in step (I), and (III) solution treatment at 1080°C for 30 min and then air cooling to room temperature followed by direct aging as described in step (I).

### Characterizations of the Joints

The microwave induced welded joints and post-heat-treated joints were cut across the welding direction using a 200- $\mu\text{m}$  slow speed diamond cutter (Chennai Metco, Tamil Nadu, India). The welded specimens were polished according to standard metallographic procedures, and the polished specimens were etched by Kalling's reagent (50 mL methanol, 50 mL hydrochloric acid, and 2.5 g cupric chloride). The microstructural features of the joint zone were studied using FE-SEM and an optical microscope. The average Nb concentrations at the joint zone in the interdendritic regions and dendritic regions were carried out using an energy-dispersive x-ray detector (Quanta 200 FEG; FEI Company, Hillsboro, OR). Microhardness measurements were carried out across the joint zone using a Vickers microhardness tester at a testing load of 25 g for a dwell time of 10 s (Chennai Metco). Room-temperature tensile properties of the welded specimens were determined on a computer-controlled universal testing machine at an extension rate of 0.2 mm/s (Instron Corporation, Norwood, MA) as per the ASTM standard. The failure mode of the fractured surfaces of the joints was determined using SEM micrographs to determine the structure–property–fracture correlations.

**Table II. Microwave processing parameters used for joining Inconel 718 plates**

Parameters	Description
Applicator	Industrial microwave oven
Base material	Inconel 718 plates
Frequency	2.45 GHz
Interfacing powder layer	Inconel 718 powder in slurry form
Susceptor material	Charcoal powder
Flux material	UV 420 TT
Exposure power	1.1 kW
Exposure time	540 s

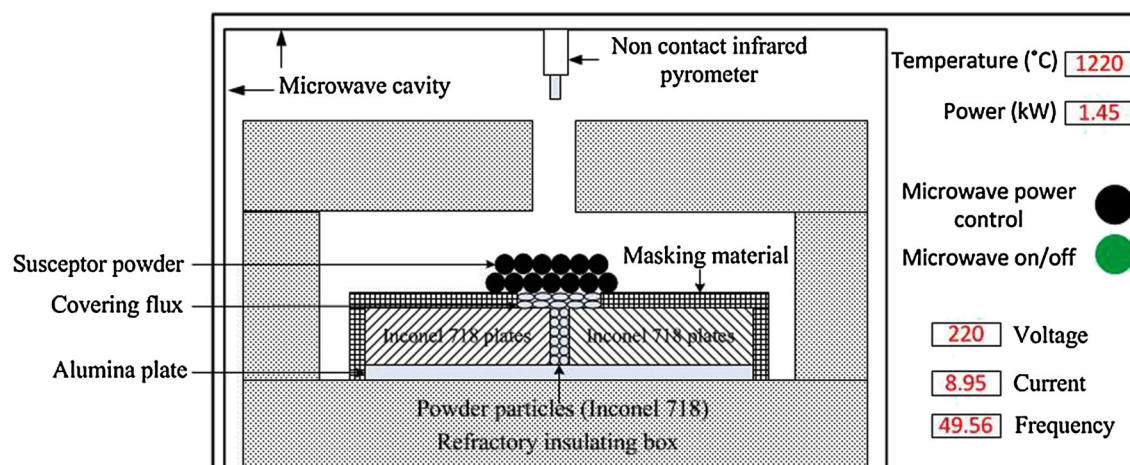


Fig. 5. Schematic diagram of the MHH setup used for joining of Inconel 718 plates (Color figure online).

## RESULTS AND DISCUSSION

The characterization results of the as-welded joints and post heat-treated joints while subjected to various test environments are discussed with suitable illustrations in the following sections.

### Joint Zone Microstructure

Figure 6 represents the back-scattered electron (BSE) micrographs of the fusion zone of the joints developed by MHH technique. There is no evidence of any sign of microfissure (microcracks) as well as macrocracks in the joint zone. The microfissure-free joint was formed due to volumetric heating associated with the MHH process. The as-welded joints as shown in Fig. 6a were characterized by precipitation of intermetallic phases, including Laves phase and MC carbides in the interdendritic regions of the fusion zone as a result of segregation of high-concentration refractory elements such as Nb and Mo. The formation of Laves phase in Inconel 718 can be explained as follows. Solidification in alloy 718 starts with the primary  $L \rightarrow \gamma$  reaction and

proceeds by enrichment of interdendritic liquid with Nb, Mo, Ti, Si, and C elements. The subsequent  $L \rightarrow (\gamma + NbC)$  eutectic type of reaction occurs, and it terminates the solidification process. Thus, the formation of Laves phase is due to the segregation of Nb in the interdendritic regions, and it is an unavoidable terminal solidification phase in alloy 718. Figure 6b represents the fusion zone microstructure in STA/aged condition and Fig. 6c and d represent the fusion zone microstructures in STA/981STA, and STA/1080STA conditions, respectively. The contrast between the Nb-rich regions are brighter than the matrix because of the relatively higher atomic weight of Nb. The Laves phase is detrimental to the weld mechanical properties because they are hard and brittle in nature. Once the Laves phase is formed in the matrix, the only way to get uniform microstructure is to redissolve the Laves phase back into the matrix using solutionizing heat treatment. The direct aging treatment did not dissolve any Laves phase in the matrix (Fig. 6b). This treatment is only designed for the precipitation of strengthening phases ( $\gamma'$ ,  $\gamma''$ ) in the matrix. The 981STA

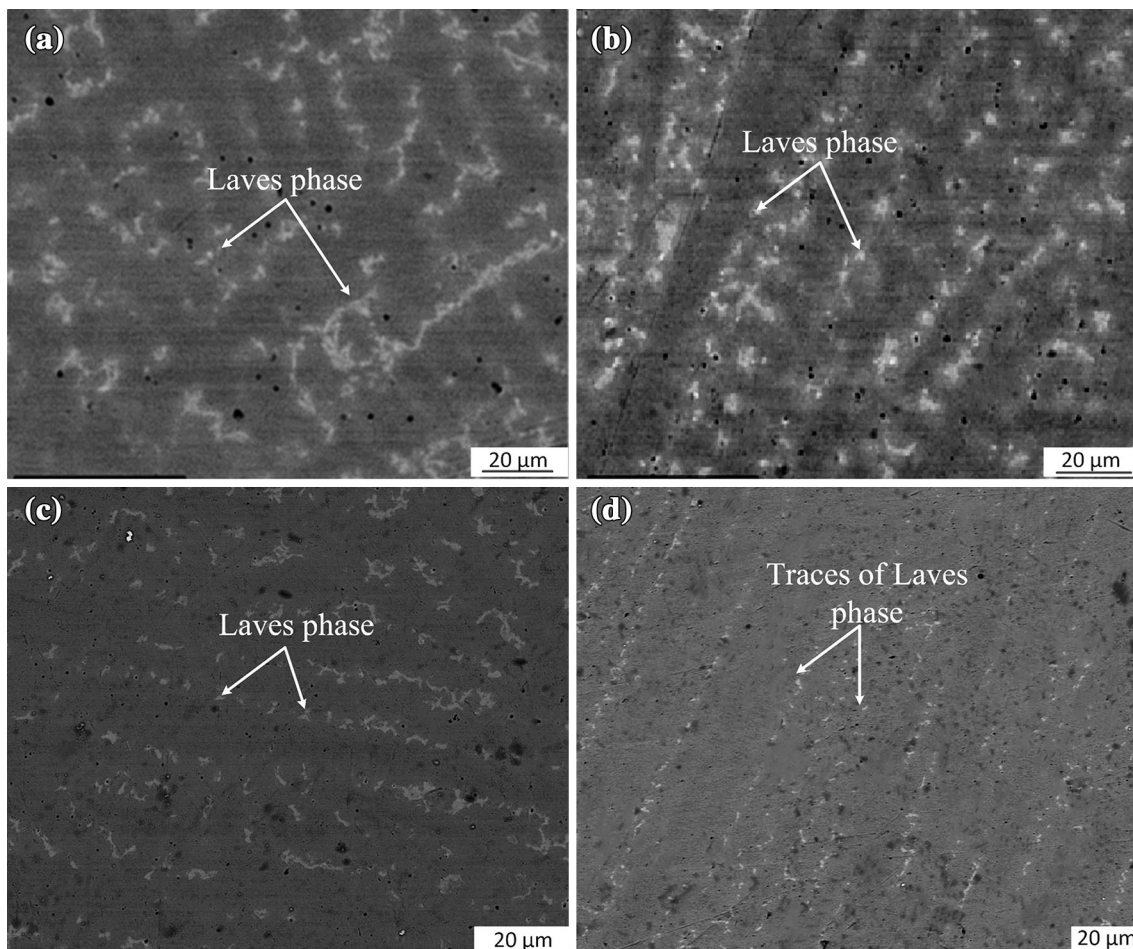


Fig. 6. BSE micrographs of the joint zone at (a) STA/as-welded condition, (b) STA/aged condition, (c) STA/981STA condition, and (d) STA/1080STA condition.

results in the partial dissolution of the Laves phase in the matrix as shown in Fig. 6c. On the other hand, the 1080STA treatment results in an almost complete dissolution of Laves phase in the matrix and only traces of Laves phase were left after this treatment (Fig. 6d). Thus, following the 1080STA treatment, most of the Laves phase was completely dissolved in the matrix, and an almost isotropic microstructure with recrystallized large grains was formed. However, the MC carbides are relatively stable phases at high temperature, and they remain in the matrix and the grain boundaries after this treatment.

### Elemental Analysis Results

To determine the elemental composition in various weld joints developed through MHH, the quantitative elemental distribution in the interdendritic regions and dendritic regions of the welded zone was carried out using x-ray elemental map analysis. The results of elemental mapping are presented in Table III. It has been found that interdendritic core regions are highly depleted of Nb (~26%) compared with base metal (~5%) in the case of as-welded joints. A similar trend has been observed for Ti and Mo, but to a lower extent than Nb. Because Nb, Mo, and Ti have higher atomic weight elements, they segregate more than other elements. Although there is an enrichment of Nb, Mo, and Ti in the interdendritic regions, the same was depleted of nickel, iron, and chromium. The as-welded and aged specimen has exhibited almost the same segregation of Nb (~26%) in the interdendritic regions as in the as-welded specimen (~26%). The 981STA weld metal has also significant segregation of Nb in the interdendritic regions (~18.91%) compared with the base metal (~5%), but it has less segregation of Nb than the as-welded and as-welded and aged specimens. On the other hand, the 1080STA specimen has almost negligible segregation of Nb (~5%) in the interdendritic regions compared with the base metal (~5%). The 1080STA treatment results in the effective homogenization of the weld structure; thus, this treatment evened out the compositional difference of the all alloying elements in the weld metal. The BSE images of the fusion zone at higher magnifications

are shown in Fig. 6a–d and the corresponding Nb x-ray mapping of the fusion zone are shown in Fig. 7a–d. The microsegregation of Nb, and as a result of which the formation of Laves phase, is governed by the weld cooling rate and heat input. The slow cooling rate generally results in relatively large dendrite arm spacing compared with rapidly cooled welds; these dendrite arm spacings are the preferred sites for segregation of alloying elements during solidification. Although the flux used in the experimentation prevents the oxidation of interfacing surfaces at a high temperature, it significantly reduces the weld cooling rate, which causes the segregation of Nb, Mo, and Ti; hence, the formation of Nb-rich Laves phase occurred. The distribution of elements across the Laves phase was further determined through elemental line scanning as shown in Fig. 8a, and the corresponding distribution of elements were superimposed across the line scanning area as shown in Fig. 8b. It is clear from Fig. 8b that the Laves phase has a higher percentage of Nb, Mo, Ti, and Si, and the same was depleted by Ni, Fe, and Cr.

### Microhardness Study

Microhardness of the MHH-induced welded joints were measured across the joints and on either side of the base metal using a load of 25 g applied for a duration of 10 s. The typical microhardness profile is plotted in Fig. 9 and average values of the hardness are given in Table IV. The base material used in the current study in 981STA condition has average microhardness of 475 HV. For STA/as-welded joints (Table IV), the fusion zone has considerably lower hardness than that in base metal. The lower microhardness in the fusion zone was attributed to the fact that the principal strengthening phase  $\gamma''$  gets dissolved in the fusion zone due to the rapid weld thermal cycle that occurred during MHH process. The aging treatment or full heat treatment (solution treatment or aging) will restore the microhardness due to reprecipitation of strengthening phase (both primary as well as secondary) in the fusion zone. In STA/aged specimen (Table IV), relatively higher microhardness was observed in the fusion zone than in the as-welded

**Table III. Elemental analysis results of the MHH developed joint**

Workpiece	Regions	Nb	Mo	Ti	Ni	Cr	Fe
Base metal	Matrix	5.14	2.56	0.84	52.55	17.92	19.62
As-welded specimen	Interdendritic	26.72	2.81	2.41	36.45	14.56	15.68
	Dendritic core	2.75	1.95	0.27	47.70	24.96	21.02
As-welded and aged specimen	Interdendritic	26.42	2.61	2.31	37.10	14.36	15.43
	Dendritic core	2.65	2.05	0.24	46.73	23.85	22.13
As-welded and 981STA specimen	Interdendritic	18.91	2.01	1.80	45.28	15.60	15.19
	Dendritic core	3.45	2.92	0.20	54.59	19.14	17.80
As-welded and 1080STA specimen	Interdendritic	5.22	3.08	0.54	52.08	18.75	18.06
	Dendritic core	4.96	2.90	0.39	52.54	18.53	18.29

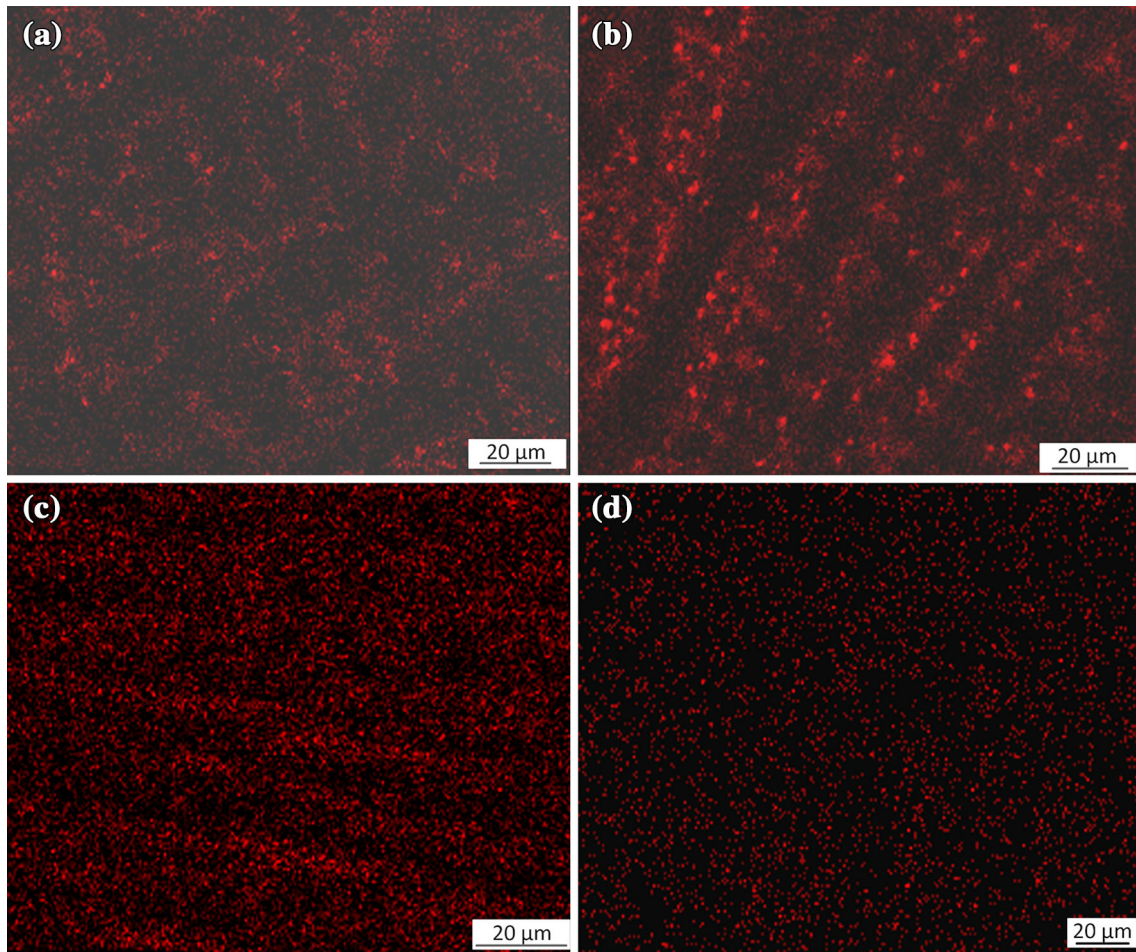


Fig. 7. Niobium x-ray mapping in (a) STA/as-welded condition, (b) STA/aged condition, (c) STA/981STA condition, and (d) STA/1080STA condition.

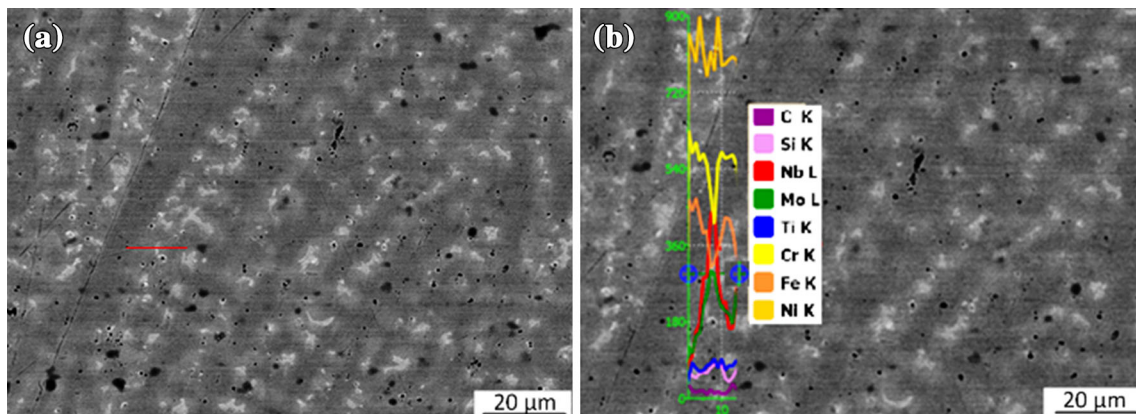


Fig. 8. BSE micrographs indicates the (a) location of the line scanning area (red line) and (b) superimposed distribution of elements across the line scanning area (Color figure online).

fusion zone due to precipitation of strengthening precipitates in the microstructure. The STA/981STA specimen (Table IV) has higher hardness in the fusion zone than in the as-welded and as-welded/aged specimens. This is attributed to the

fact that the 981°C solution treatment results in considerable dissolution of Laves phase in the fusion zone. The Laves phase present in the fusion zone consumes most of the alloying elements, mainly Nb; the principal strengthening phase is



required for desired hardness and strength. The dissolution of the Laves phase releases Nb, which increase the reprecipitation of  $\gamma''$ ,  $\gamma'$  and lead to an increase of the hardness and strength of the fusion zone. These coherent precipitates ( $\gamma''$ ,  $\gamma'$ ) produce coherency strains in the matrix, which results in an increase in hardness and tensile strength of the joints. Also, the temperature required in 981°C solution treatment is less than the solvus temperature of orthorhombic delta phase ( $\delta\text{Ni}_3\text{Nb}$ ), which precipitates in the interdendritic regions and grain boundaries in the matrix and it prevents the grain coarsening of the matrix. The solvus temperature of the orthorhombic delta phase ( $\delta\text{Ni}_3\text{Nb}$ ) is approximately 995°C.<sup>3</sup> The STA/1080STA fusion zone

(Table IV) has higher microhardness among all the welded conditions. This is due to fact that after the 1080STA treatment, the Laves phase got almost completely dissolved in the matrix and only traces of the Laves phase were left after this treatment. But the 1080STA-treated base metal has lower microhardness than that in 981STA-treated base metal because the temperature required in 1080°C solution treatment was greater than the solvus temperature of orthorhombic delta  $\text{Ni}_3\text{Nb}$  phase and it results in formation of recrystallized large grains, which severely deteriorate the mechanical properties of the material and alloy.

### Observations on Tensile Strength and Fractography Study of the MHH-Induced Welded Joints

The specimens were tested at room temperature in a computer-controlled universal testing machine with an extension rate of 0.2 mm/s. The specimens were prepared according to ASTM standard with 18 mm gauge length and width of 3.5 mm. A schematic diagram of the standard tensile specimen is shown in Fig. 10a and an optical micrograph of one of the prepared tensile specimen is shown in Fig. 10b. The results are summarized in Table V for base metal as well as welded specimens in various heat-treated conditions. It is observed from Table V that the tensile strength of base materials in 1080STA condition is considerably lower than that in 981STA condition, but it has a higher percentage of elongation than that in 981STA due to grain coarsening that took place after 1080STA heat treatment. It is observed from Table V that the lowest ultimate strength and highest percentage elongation was achieved for STA/as-welded condition. This is due to fact that the strengthening phases were dissolved in the fusion zone after rapid weld thermal cycle involved in MHH process and a relatively soft matrix will be formed. On the other hand, the STA/aged specimen has the lowest percentage of elongation among all welded conditions due to the presence of both coherent precipitate ( $\gamma'$ ,  $\gamma''$ ) and brittle Laves phase in the joint zone. The aging treatment or full heat treatment (solution treated and aged) results in an increase in tensile strength due to reprecipitation of strengthening phases (primary and secondary phases) in the joint zone. The higher tensile strength was achieved for STA/981STA condition followed by STA/aged

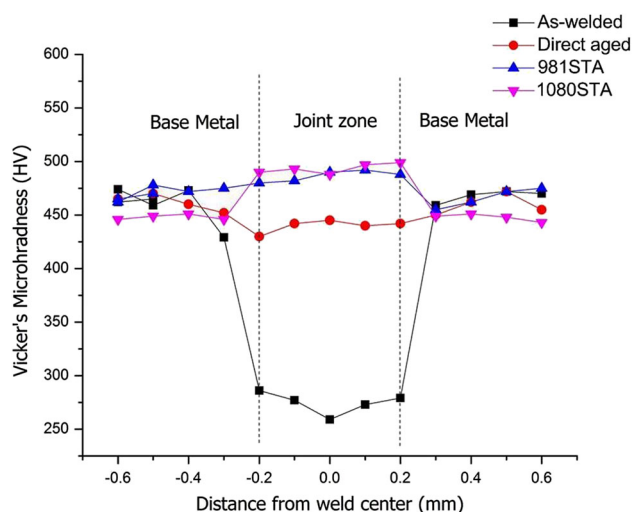


Fig. 9. Distribution of the Vicker's microhardness under different heat-treatment conditions.

**Table IV. Average microhardness (HV) values for the different welding conditions**

Preweld and postweld heat treatment	Fusion zone	Base metal
STA/as welded	248 ± 15	470 ± 12
STA/aged	440 ± 10	473 ± 10
STA/981STA	480 ± 5	475 ± 5
STA/1080STA	485 ± 6	470 ± 10

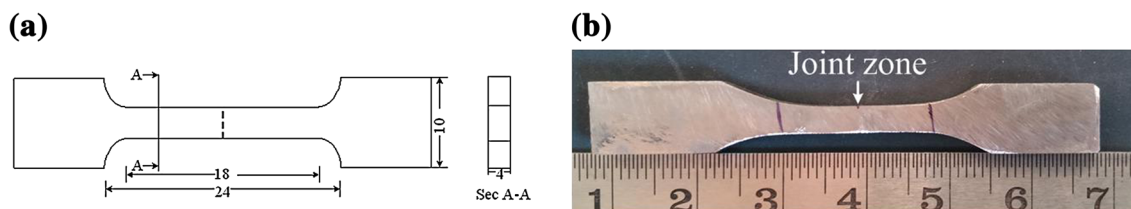


Fig. 10. (a) A schematic of typical tensile test specimen. (b) Optical micrograph of the tensile test specimen.

condition followed by STA/1080STA and then followed by STA/as-welded condition. However, there is a marginal increase in tensile strength in the STA/981STA condition compared with STA/aged condition. This indicates that the full heat treatment (solution treated and aged) is not required for getting the desired tensile strength in the joint, and only the aging heat treatment is good enough to strengthen the weld. The aging treatment causes relief of welding residual stresses, improving stress corrosion and reduced weld distortion. This treatment also prevents grain coarsening that would take place after the full heat-treatment condition. The results are in agreement with Cao et al.,<sup>10</sup> who reported that postweld aging heat treatment was enough to strengthen the weld instead of fully heat treated condition (solution treated and aged). The optical micrographs of the fractured specimens in each welding condition are shown in Fig. 11. All welded specimens failed in the joint zone except the joint formed in the 1080STA condition. The 1080STA-welded specimen had failed at the base metal, which indicated that the weld metal in the 1080STA condition is as strong as that of the base metal. Similar results were reported by Ram et al.<sup>11</sup>

The fractured specimens for each welding condition were cleaned with acetone in the ultrasonic cleaner for 15 min for fractography study. The SEM images of the fractured specimens were obtained in

the secondary electron mode. The SEM images of the fractured surfaces for each welding condition are given in Fig. 12. In each image, the protrusion of phases was observed inside the dimple. To determine the composition of these phases, the EDS spectra were taken inside the dimple (protrusion phase) and its outer edge as seen in Fig. 12e and f corresponds to the marked position in Fig. 12a. It has been observed from EDS spectra that the protruded phases were mainly enriched in Nb, Mo, and Ti. Thus, these protruded phases were mainly Laves phase, which segregates in the interdendritic regions during the welding process. The fractured surfaces of the STA/as-welded specimen show a dimple indicating a ductile failure. The fractured surfaces of the as-welded and aged specimen show the morphology of the mixed mode of failure; the brittle mode of failure was due to the presence of incoherent Laves phase. As the load is applied, the matrix tends to deform plastically, but Laves phase is inherent and brittle in nature. These phases were not deformed plastically because of their higher yield strength. As the loading continues, there is a breakdown of slip incompatibility at the incoherent particle interfaces. As a result of this, the small cavity or microvoids were formed at the interface between these phases (Laves and incoherent particles) and the matrix. These microvoids enlarge, come together, and coalesce to form cracks and finally failure of material occurred by propagation of cracks with increased loads. The fractured surfaces of 981STA treatment show a dendritic pattern with dimpled fracture feature due to partial dissolution of Laves phases after treatment. This indicates that fracture took place mainly along the interdendritic regions and was a ductile failure. On the other hand, the fractured surfaces in 1080STA treatment show completely dimple fractured feature because the failure took place in the base material and the Laves phase are completely dissolved after this treatment. The size and shape of the dimples in the fractured surfaces for each welding condition are related to the size, shape, and dispersion of  $\gamma'$  and  $\gamma''$  precipitates in the matrix. The size of the dimple is

**Table V. Room-temperature tensile strength results**

Preweld and postweld heat treatment	UTS (MPa)	Elongation (%)
Base material in 981STA	1392	14
Base material in 1080STA	1355	16.67
STA/as-welded specimen	798.39	11.97
STA/aged specimen	1274.81	7.8
STA/981STA specimen	1283.38	8.27
STA/1080STA specimen	1267	9.99

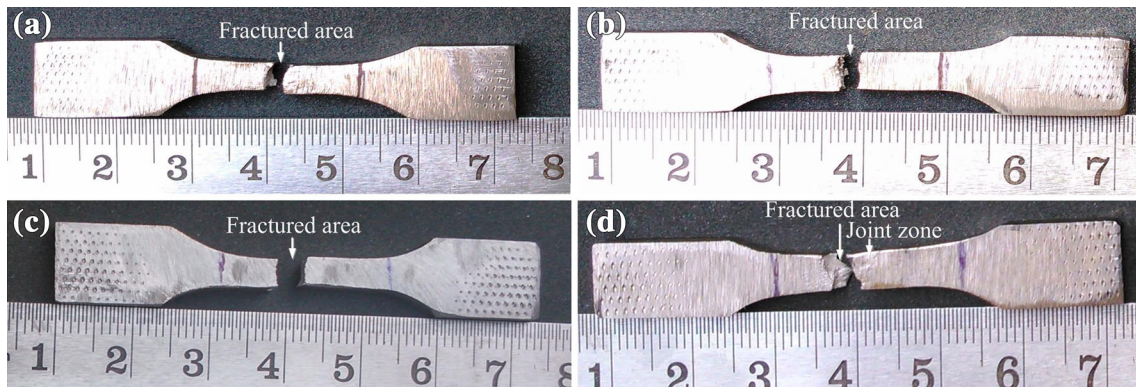


Fig. 11. Optical micrographs of the fractured specimens in (a) STA/as-welded condition, (b) STA/aged condition, (c) STA/981STA condition, and (d) STA/1080STA condition.

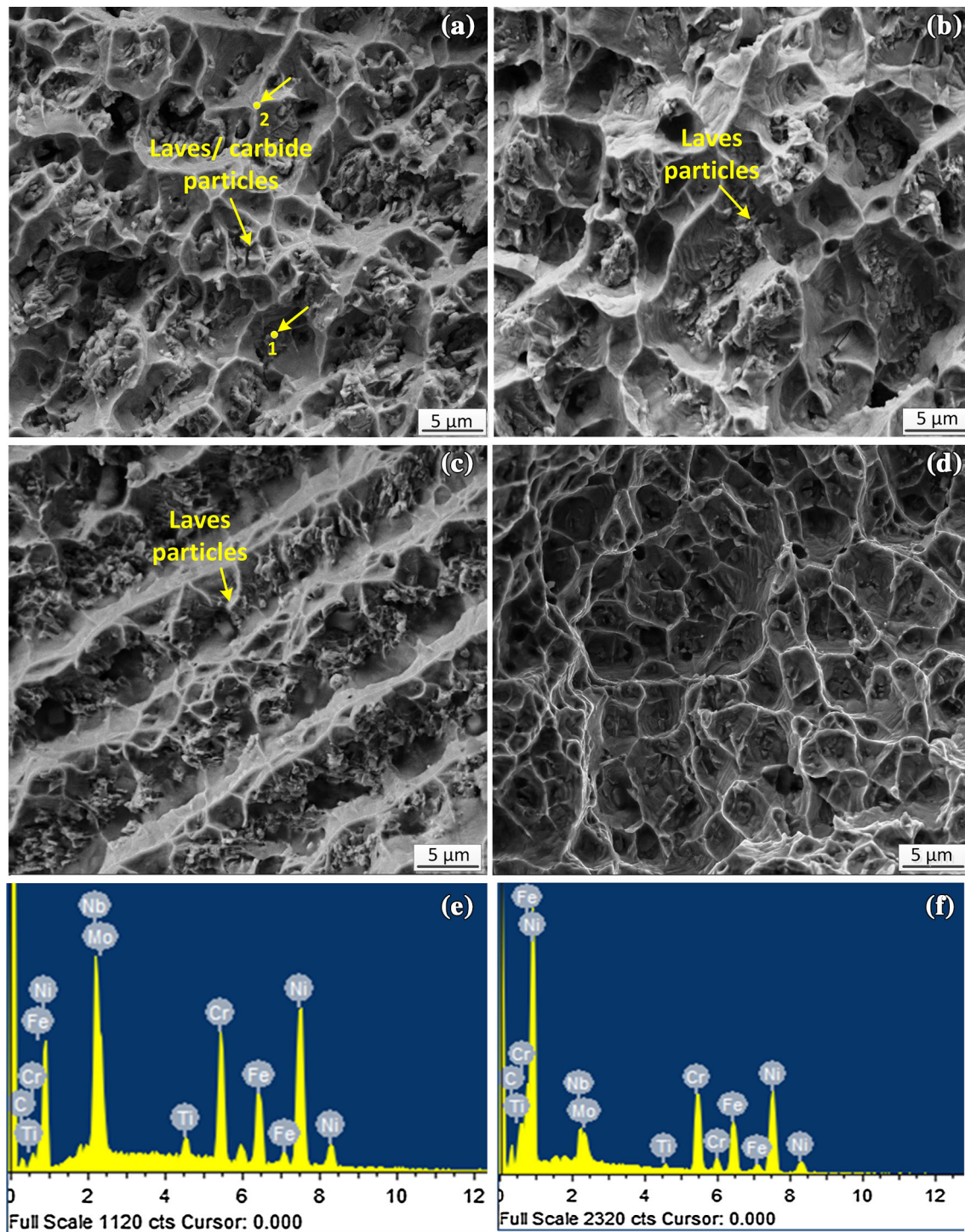


Fig. 12. SEM images of the fractured surfaces at (a) STA/as-welded specimen, (b) STA/aged specimen, (c) STA/981STA specimen, (d) STA/1080STA specimen, and (e, f) EDS spectra at marked positions 1 and 2 corresponding to STA/as-welded condition.

also related to the strength of the alloy and its temperature.

### CONCLUSION

In the current work, butt joining of Inconel 718 has been accomplished through the principles of MHH. The postweld heat treatment of the as-welded

joints was carried out for improving their microstructure and mechanical properties. The major conclusions drawn from the present work are as follows:

1. The principles of MHH were successfully applied for butt joining of Inconel 718 plates. The developed joints are metallurgically bonded to

either side of base material through complete melting of powder particles.

2. The joints are free from any microfissure or crack due to uniform heating associated with MHH process.
3. The postweld heat treatment improves the mechanical properties of material by precipitation of strengthening phases in the matrix. Compared with as-welded, the direct aged heat treatment did not result in any change in the microstructure of the joint in terms of the Laves phase present in the matrix. The 981STA treatment dissolves a large amount of Laves phase in the matrix, which increases the ductility and strength of the joint.
4. After 1080STA treatment, the Laves phase is almost completely dissolved in the matrix, but significant grain growth took place after this treatment, which deteriorates the mechanical properties including tensile strength and hardness of the base material.
5. Microhardness of the fusion zone of joint is higher in 1080STA treatment followed by 981STA treatment followed by direct-aged heat treatment and then followed by as-welded joint.
6. The postweld aging treatment is optimal to strengthen the weld instead of the fully heat-treated condition (solution treated and aged). However, there is a marginal increase in tensile strength in STA/981STA condition compared with the STA/aged condition. But the full heat treatment (solution treated and aged) is not preferred because this treatment consumes more energy and causes distortion of the welded specimen. Moreover, the full heat treatment results in grain coarsening of materials, which deteriorates the mechanical properties of base material.

## ACKNOWLEDGEMENT

The authors would like to express gratefulness to the Board of Research of Nuclear Sciences (BRNS) India for financing this work with Project No. 2010/36/60-BRNS/2048.

## REFERENCES

1. A. Lingenfelte, *Welding of Inconel 718—A Historical Review 1989*, ed. E.A. Loria (Warrendale, PA: TMS, 1989), pp. 673–683.
2. S. Kou, *Welding Metallurgy*, 2nd ed. (Hoboken, NJ: Wiley, 2003), pp. 375–392.
3. G.D.J. Ram, A.V. Reddy, K.P. Rao, and G.M. Reddy, *Mater. Sci. Technol.* 21, 1132 (2005).
4. C. Slama, and M. Abdellaoui, *J. Alloy. Compd.* 306, 277 (2000).
5. D.F. Paulonis, J.M. Oblak, and D.S. Duvall, *Trans. ASM* 62, 611 (1969).
6. G.D.J. Ram, A.V. Reddy, K.P. Rao, and G.M. Reddy, *Sci. Technol. Weld. Join.* 9, 390 (2004).
7. N.L. Richards, X. Huang, and M.C. Chaturvedi, *Mater. Charact.* 28, 179 (1992).
8. C.H. Radhakrishna and K.P. Rao, *Mater. High Temp.* 12, 323 (1994).
9. C.H. Radhakrishna and K.P. Rao, *J. Mater. Sci.* 32, 1977 (1997).
10. X. Cao, B. Rivaux, M. Jahazi, J. Cuddy, and A. Birur, *J. Mater. Sci.* 44, 4557 (2009).
11. G.D.J. Ram, A.V. Reddy, K.P. Rao, G.M. Reddy, and J.K.S. Sundar, *J. Mater. Process. Technol.* 167, 73 (2005).
12. S. Gobbi, L. Zhang, J. Norris, K.H. Richter, and J.H. Loreau, *J. Mater. Process. Technol.* 56, 333 (1996).
13. W.H. Suttan, *Am. Ceram. Soc. Bull.* 168, 376 (1989).
14. D. Gupta and A.K. Sharma, *Surf. Coat. Technol.* 205, 5147 (2011).
15. R. Roy, D. Agrawal, J. Cheng, and S. Gedevisanishvili, *Nature* 399, 668 (1999).
16. A.K. Sharma, M.S. Srinath, and P. Kumar, Indian patent 1994/Del/2009 (2009).
17. M.S. Srinath, A.K. Sharma, and P. Kumar, *J. Manuf. Process.* 13, 141 (2011).
18. M.S. Srinath, A.K. Sharma, and P. Kumar, *Mater. Des.* 32, 2685 (2011).
19. M.S. Srinath, A.K. Sharma, and P. Kumar, *Proc. Inst. Mech. Eng. B J. Eng. Manuf.* 225, 1083 (2011).
20. R. Vincent, *Acta Metall.* 33, 1205 (1985).